SCIENTIFIC REPORTS

SUBJECT AREAS:
SPINTRONICS
FERROMAGNETISM
MAGNETIC PROPERTIES AND MATERIALS
ELECTRONIC PROPERTIES AND MATERIALS

Received
11 February 2013

Accepted
2 May 2013

Published
6 June 2013

Correspondence and requests for materials should be addressed to W.G.W. (wgwang@physics.arizona.edu) or C.L.C. (clc@pha.jhu.edu)

* Current address: Department of Physics, University of Arizona, Tucson, AZ 85721, USA.

Parallel fabrication of magnetic tunnel junction nanopillars by nanosphere lithography

W. G. Wang*, A. Pearse, M. Li, S. Hageman, A. X. Chen, F. Q. Zhu & C. L. Chien

Department of Physics and Astronomy, The Johns Hopkins University, Baltimore, Maryland 21218, USA.

We present a new method for fabricating magnetic tunnel junction nanopillars that uses polystyrene nanospheres as a lithographic template. Unlike the common approaches, which depend on electron beam lithography to sequentially fabricate each nanopillar, this method is capable of patterning a large number of nanopillars simultaneously. Both random and ordered nanosphere patterns have been explored for fabricating high quality tunneling junctions with magnetoresistance in excess of 100%, employing ferromagnetic layers with both out-of-plane and in-plane easy axis. Novel voltage induced switching has been observed in these structures. This method provides a cost-effective way of rapidly fabricating a large number of tunnel junction nanopillars in parallel.

The evolution of microelectronics, which has adhered closely to Moore's law[1] for over four decades, will soon face formidable obstacles. Among many serious challenges are issues due to the large leakage current of next generation CMOS transistors in the off-state, caused by the reduction of gate oxide thickness in sub-20 nm transistors[2]. One attractive alternative is to exploit spin-based nonvolatile devices that intrinsically consume no power in the off-state[3,4]. In this regard, magnetic tunnel junctions (MTJs) offer the best prospects[5–8]. The basic structure of an MTJ consists of two ferromagnetic (FM) thin films separated by an ultrathin insulating layer. The high and low resistance states of an MTJ depend on the relative orientations of the two FM layers being antiparallel and parallel, respectively. The resistance difference between the two states defines the tunneling magnetoresistance (TMR) value of an MTJ. The MTJs with MgO barriers exhibiting very large TMR are widely recognized as the best candidates for magnetic random access memory (MRAM) and spin logic applications[9]. The spin transfer torque (STT) effects that enable site-specific current switching, as opposed to proximity field switching, have been extensively explored, although the switching current density remains too high[10–13]. Very recently, voltage induced switching in MTJs has been realized[14,15], demonstrating a promising way to achieve ultralow energy switching.

The growth of MgO-MTJs is very demanding, requiring a high quality MgO barrier and precise matching of electronic bands to capture the giant TMR[16]. The fabrication of high quality MTJ nanopillars for pursuing STT or voltage induced switching is even more challenging due to the complex procedure and advanced instrumentation involved. The most common technique employed in fabricating MTJ nanopillars is electron beam lithography (EBL), by the top down[17–21] or stencil approaches[22,23], although other techniques such as deep-ultraviolet photolithography[24] and focused ion beam[25] have also been used. In the EBL-based procedure, the nanostructures are defined by an electron beam in a sequential manner, which is intrinsically very time consuming and limited to small scales. The complex fabrication protocols, often including multiple steps of EBL, rely on advanced and not coincidently expensive instruments. The challenging fabrication process impedes study and exploration of nanoscale MgO-MTJs despite their promising prospects.

In this work, we describe a new method for the fabrication of high quality MTJ nanopillars using nanosphere lithography (NSL)[26–29], which is inherently parallel, capable of patterning a large number of nanopillars simultaneously. The nanospheres serve the dual purposes of etching mask for defining nanopillars, as well as self-aligned lift-off mask for removing the insulation layer on top of nanopillars. As a result, the fabrication time can be greatly reduced. More importantly, this approach requires no EBL or other expensive fabrication tools. In the past nanospheres have been successfully used to create contacts for the metallic spin torque oscillators through hole mask colloidal lithography[30], where the shape of the metallic oscillators were defined by a metal layer transferred from the nanosphere. Here in our method the shape of the MTJs is directly defined by nanospheres. This new

NSL-based method may greatly facilitate research on MTJ nanopillars including the exploration of the ultralow energy magnetization switching.

Results

The essential steps of this fabrication method are schematically shown in Fig. 1, involving three photolithography processes and one NSL process. First, blanket multilayer thin films of the constituent layers of MTJs are deposited on a Si wafer. The multilayer films are grown in a UHV magnetron sputtering system. More details on sample growth are presented in the supplementary section. The first photolithographic step with subsequent ion beam etching defines the base mesa structure of a 2 μm-wide line connecting two large contact pads (200 μm × 200 μm) as shown in Fig. 1a. For illustrative purpose we consider the simplest MTJ consisting of two FM electrodes separated by a thin tunneling barrier of MgO. We stop the ion beam etching at the top of the Si wafer. The second photolithographic step deposits photoresist pads with the exact size (200 μm × 200 μm) to protect the two bottom contact pads from the SiO_2 deposited afterwards. We next employ NSL to place monodispersive polystyrene nanospheres of a specific diameter with a desired density on the top of the entire wafer. This is accomplished by placing an excessive amount of positive charge on the wafer through chemical treatment. After submerging the treated wafer into the nanosphere solution, the negatively charged nanospheres are then deposited with a density dictated by the concentration of the nanosphere solution and the dwell time (Fig. 1b). A uniform but random nanosphere coverage over a large area of several square inches can be readily accomplished. The nanospheres deposited on the 2-μm line serve as the hard masks to define the size of the nanopillars during the ion beam etching process. We stop the etching right at the MgO tunnel barrier layer (Fig. 1c). Next, a SiO_2 insulating layer is deposited over the entire wafer, electrically isolating the top and the bottom electrodes of the MTJ pillars (Fig. 1d). Due to the good mechanical strength, the nanospheres also function as self-aligned mask for the SiO_2 lift off, which exposes only the top of each nanopillar while the rest structures are covered by SiO_2 (Fig. 1e). We then use the third photolithography step to pattern a series of 2-μm lines that are orthogonal to the 2-μm wire of the base mesa structure. The top contact pads are created by depositing and lifting-off a Ta/Au bilayer (Fig. 1f). The illustration in Figure 1 only shows one dumbbell-shape base mesa with six pair of top contact pads. In practice, a large quantity of such structure can be fabricated, providing thousands or even more of nanopillars on a single wafer.

Scanning electron microscopy (SEM) micrographs of samples during various stages of the fabrication process are shown in Fig. 2. The core structure of the MTJs is $Co_{40}Fe_{40}B_{20}$(1.2 nm)/MgO(0.9–1.4 nm)/$Co_{40}Fe_{40}B_{20}$(1.7 nm). The diameter of the nanosphere used in NSL is 400 nm. The wafer with bottom mesa structures has been first treated in aluminum chloride hydroxide solution for 20 s to carry a layer of positive charges. Then nanospheres are deposited by submerging the wafer in a 0.025% (by weight) nanosphere solution for 10 s. The distribution of the nanospheres over the wafer is shown in Fig. 2a, including the 2 μm wire of the base mesa structure. One critical step of this fabrication procedure is to minimize damage to the nanospheres during ion beam etching to ensure successful lift off afterwards. We have used a low Ar^+ beam density of 0.2 mA/cm^2 at an Ar pressure of 0.2 mTorr. The circular shape of the nanosphere is precisely transferred to the MTJ nanopillar as shown in Fig. 2b with a very sharp edge. We have deposited an 85 nm SiO_2 insulating layer at 1.2 mTorr, at which SiO_2 goes slightly under the nanospheres, thus completely covering the MTJ structure below the MgO barrier. The subsequent lift-off of the nanosphere created an opening of about 370 nm at the top, as shown in Fig. 2c. The third photolithography step then patterned the shape of top electrodes (Fig. 2d), which are created by liftoff of the Ta(10 nm)/Au (150 nm) bilayer as shown in Fig. 2e. At this point, complete MTJ nanopillars have been fabricated on a wafer all with 4 contact pads, as shown in Fig. 2f, await subsequent thermal annealing and measurements[31–34].

The intersection of the top Ta/Au electrode and the bottom mesa structure forms a 2 μm × 2 μm cell. Each cell has two top contact pads and two bottom contact pads (shared) for the 4-probe measurement. For a given distribution of nanospheres, there is a specific probability for having a certain number of nanopillar(s) present in a 2 μm × 2 μm cell. We have tested 200 such 2 μm × 2 μm cells patterned on a blanket film with a wedge-shaped MgO barrier (0.95 nm – 1.35 nm). About half of the 200 cells showed open-circuit ($R > 10^7\ \Omega$), indicating no nanopillar in these cells. For the

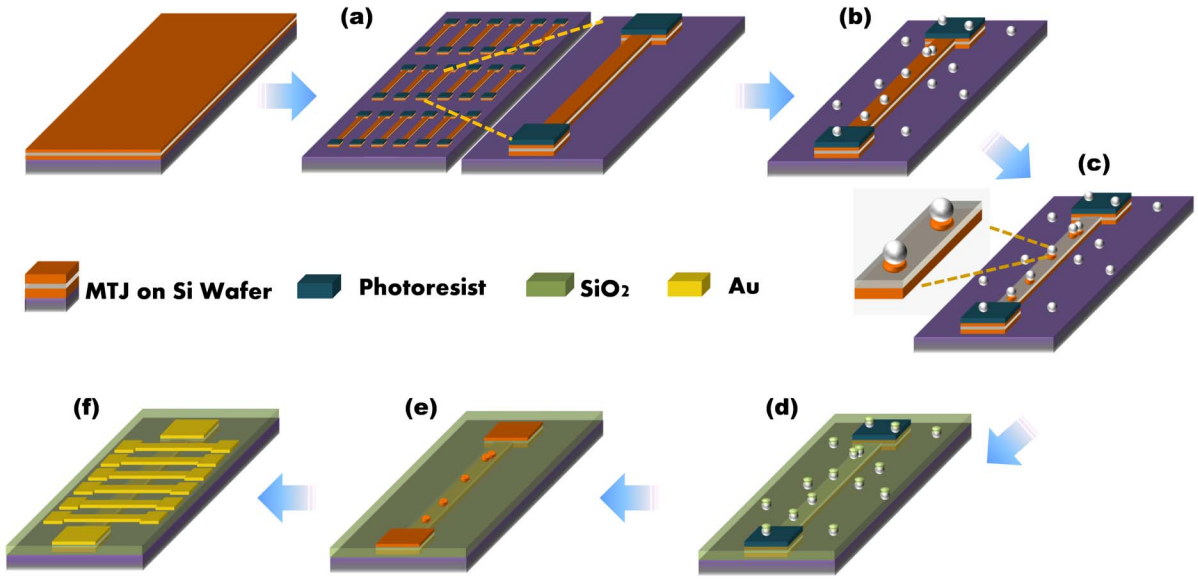

Figure 1 | Schematic fabrication procedure of MTJ nanopillars using NSL. (a) Bottom mesa structures are created from the blanket MTJ film by the first photolithography and ion beam etching, then the bottom contacts are protected by the second photolithography. (b) Random nanospheres are deposited on the entire wafer. (c) MTJ nanopillars are defined by the second ion beam etching. (d) SiO_2 insulating layer is deposited. (e) Nanospheres and photoresist are lifted off, exposing the contact window. (f) Complete samples with Ta/Au top electrodes.

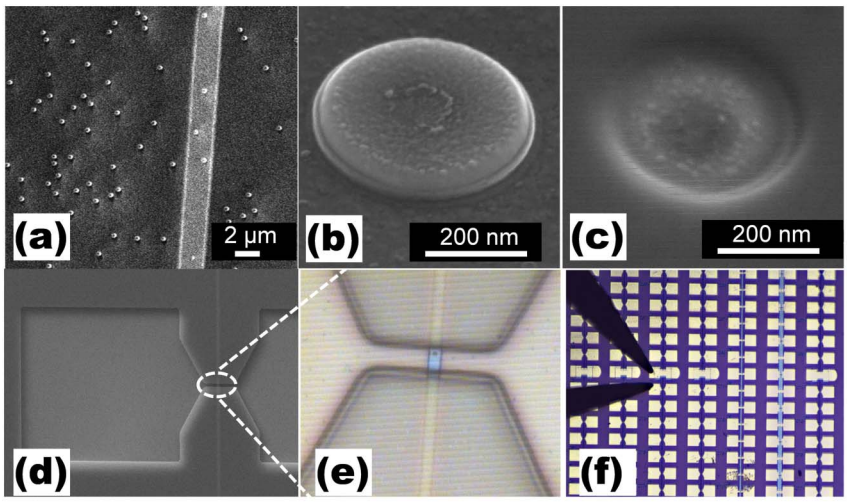

Figure 2 | Actual pictures during nanopillar fabrication. (a) 400 nm nanosphere are deposited on the wafer with base mesa structure. (b) MTJ nanopillar after the second ion beam etching (nanosphere is purposely removed for this picture to show the pillar before the deposition of SiO_2). (c) Contact window is created by lifting off the nanospheres after SiO_2 deposition. (d) Image reversal pattern created by the third photolithography, before deposition of Ta/Au bilayer. (e) After deposition and lift off of Ta/Au bilayer. (f) Fully patterned MTJ nanopillars.

rest of cells, the resistance R is shown in Fig. 3a, where Log$R$ increases linearly with the MgO thickness as expected for good MTJs. The tunneling magnetoresistance (TMR) of these MTJs are shown in Fig. 3b, where MTJs show TMR near 100% for this wafer after annealing for 10 min at 300°C, demonstrating that high quality MTJ structure has been achieved in majority of the nanopillars[32,34].

Since nanopillars are randomly distributed, it is essential to determine the number of nanopillars in each cell. This has been done in a number of ways. First, by comparing the resistance of each cell with that of micrometer-sized MTJs patterned by conventional process[35] with known resistance-area (RA) values, the effective tunneling area therefore the number of nanopillars within the cell can be determined. Second, the number of nanopillars in each cell can also be independently determined by direct imaging. For instance, for the cell with resistance of 75 kΩ, only one nanopillar is observed as shown in Fig. 2e, which agrees exactly with the expected RA value. Third, for many cells the resistance is distributed around three lines with the same slope in the Log$R$ vs d_{MgO} plot as shown in Fig. 3a. The three lines largely specify the number of pillars in each cell. For example, the resistance of the cells on the three lines are 142 kΩ, 69.8 kΩ and 47.5 kΩ at $d_{MgO} = 1.31$ nm, corresponding to cells with one, two and three nanopillars. All these independent methods yield consistent results that are plotted in Fig. 3c. For the 96 cells that are not open-circuit, 37 of them contain a single nanopillar and 25 cells contain two nanopillars. The remaining 34 cells contain 3 or more nanopillars, as well as defected nanopillars due to impurities in the

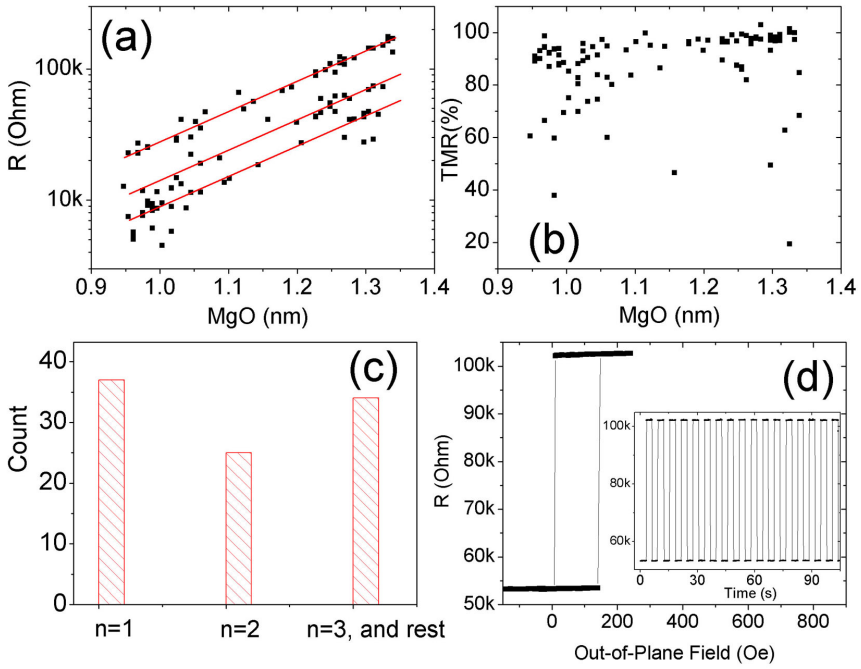

Figure 3 | (a) Distribution of resistance in 2 μm × 2 μm cells on a wafer with wedge shaped MgO barrier. The lines are guides for eyes only. (b) corresponding TMR ratios of the cells. (c) Histogram showing the counts of cells containing one, two or more nanopillars. (d) Representative TMR curve of a single-pillar cell. Inset shows the unipolar switching achieved with −0.76 V and −1.2 V pulses.

barrier, and/or back sputtering during the etching process. These results show that of the 200 cells, the yield of cells with a single nanopillar is nearly 20% for the nanosphere coverage shown in Fig. 2a. This ratio could be substantially increased with better nanosphere distribution. The cell containing more than one nanopillars may have other important applications such as synchronized microwave oscillators[36,37].

Ordered arrays of MTJs can also be fabricated, which allows a more rapid way to characterize nanopillars by directly contacting the nanopillars with a sharp conducting tip. We first place nanospheres with a desired surface charge density on top of the DI water in a Teflon cell[28]. Each nanosphere forms an electric dipole moment due to the broken inversion symmetry at the water-air interface. When the PH value (thus the ion concentration) in the water is properly adjusted, the attracting capillary force is balanced by the repulsive dipolar force, resulting an ordered structure of the nanosphere[28]. The ordered nanosphere pattern is then transferred to the blanket MTJ films. Subsequently, we use O_2 plasma to slightly reduce the size of the nanospheres, creating a small gap between the adjacent nanospheres. After the nanospheres lift-off, we have an ordered array of MTJs with the top electrodes exposed to facilitate electrical measurements of the MTJs on a probe station.

The SEM picture of an ordered MTJ nanopillar arrays is shown in Fig. 4a. This wafer was first coated with 390 nm nanospheres, whose surfaces have been functionalized by carboxyl group with parking area of 55 Å^2. Three ppm of polyethylene oxide (PEO) was added in the solution to assist the formation of ordered structure as suggested by previous study[38,39]. The wafer was then treated in O_2 plasma (see supplementary information) to reduce the size of the nanospheres from 390 nm to 300 nm. As indicated by the figure, a well ordered nanopillar array over the entire 50 μm × 50 μm area has been maintained with only a few defects. We have found that excellent ordering patterns can be achieved over an area as large as 1 cm × 1 cm, making these MTJ nanopillars arrays suitable not only for local electrical measurements, but for magnetometry characterization by VSM or SQUID as well.

Discussion

A representative TMR curve of nanopillars with contact pads is shown in Fig. 3d. This is a perpendicular-MTJs (p-MTJs), in which the two thin $Co_{40}Fe_{40}B_{20}$ layers on either side of MgO acquire perpendicular magnetic anisotropy (PMA)[21]. The TMR value of about 100% in our nanopillar is rather high among the p-MTJs. The square minor loop with high TMR ratio demonstrates the nanopillar is of high quality. The sharp switching also indicates this is a single-pillar cell as multiple steps are often seen if a cell contains more than one pillar (see supplementary information). The interfacial PMA in this MTJ can be controlled by the voltage applied to the MTJ[14]. For the top CoFeB layer, a positive (negative) voltage increases (decrease) the PMA energy. When voltages of correct polarity reduce the anisotropic energy barrier, the switching current is greatly reduced. An example of the unipolar switching by negative pulses is shown in the inset of Fig. 2d. Successive negative voltage pulses of −0.76 V and −1.2 V applied to the nanopillar every 5 s together with a constant biasing magnetic field of −50 Oe give rise to reversible voltage induced switching of p-MTJ. The details of voltage induced switching has been discussed elsewhere[14]. The p-MTJ can be reversibly and repeatedly switched by the consecutive negative pulses with average current density of only 2 × 10^4 A/cm^2, demonstrating the great potential of ultralow energy magnetization reversal in these structures.

The transport properties of ordered pillars was investigated on a probestation with a point-contact setup, where a sharp W tip, controlled by software, can approach the pillars in steps as small as 10 nm. The TMR curve is measured after the contact has been made. A close-up look of a 160-nm MTJ array and the corresponding TMR curve is shown in the inset of Fig. 4b. The core structure of these pillars is CoFeB(3 nm)/MgO(0.9 nm)/CoFeB(3 nm). The large TMR ratio and sharp switching again demonstrate the high quality of these nanopillars. Characterization of nanoscale MTJs have been carried out with conduction AFM previously[40–42], where a small number of nanopillars were fabricated by EBL. Here we can easily create billions of MTJ nanopillars over several square centimeters, with systematic variation of one or more parameters (thickness of MgO, composition of FM, etc.), thereby greatly facilitates the efficiency of MTJ characterization. The challenge in producing smaller nanopillars with stable leads lies in the lift-off of nanospheres after SiO_2 deposition and size fluctuations in sub-100 nm nanospheres, which are subjects of feature investigations.

To summarize, we have presented a high throughput, parallel fabrication method to create MTJ nanopillars over large scales up to several square inches. This method relies only on NSL and standard microfabrication procedures, without involving EBL or other expensive tools. We showed that NSL can lead to high quality MTJs, including p-MTJs with voltage-induced switching capabilities. Our technique opens a new avenue towards rapid fabrication and characterization of MTJ nanopillars for MRAM, spin logic and microwave oscillator applications.

Methods

MTJ film deposition. The tunneling junction film stacks were fabricated by a UHV magnetron sputtering system with a base pressure in the range of 10^{-9} Torr. The water vapor partial pressure, critical to the TMR and perpendicular properties of the MTJ, has been reduced by the Ta getter method as described previously[43]. All the metal layers were deposited by DC sputtering and the MgO layer was deposited by RF

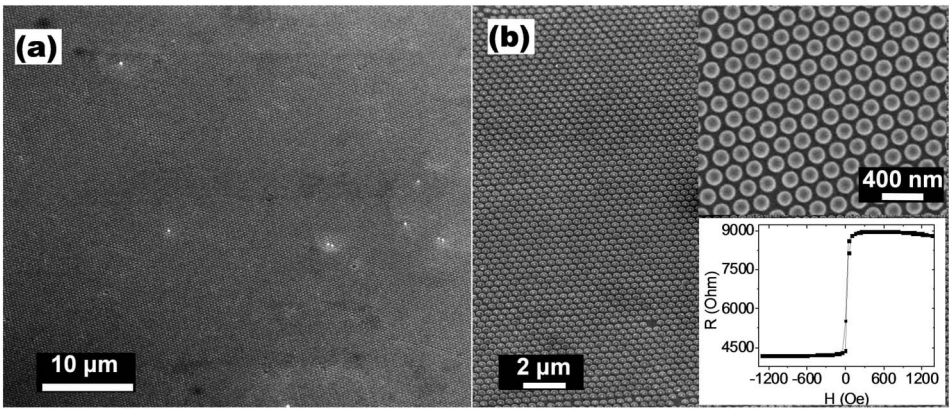

Figure 4 | (a) SEM picture of the 300 nm nanopillar array in the ordered structure. White dots are nanospheres that are not removed. (b) Close-up view of the 300 nm nanopillar array. Inset shows the 160 nm nanopillars and the corresponding TMR curve.

sputtering[31–34]. The structure of the MTJs is Si/SiO_2/buffer/$Co_{40}Fe_{40}B_{20}$(1.2 nm)/MgO(0.9–1.4 nm)/$Co_{40}Fe_{40}B_{20}$(1.7 nm)/cap for perpendicular magnetic anisotropy and Si/SiO_2/buffer/CoFe(2 nm)/IrMn(15 nm)/CoFe(2 nm)/Ru(0.8 nm)/CoFeB(3 nm)/MgO(0.9–1.4 nm)/CoFeB(3 nm)/cap for in-plane magnetic anisotropy. The buffer layer is Ta(7 nm)/Ru(15 nm)/Ta(7 nm), which is the typical structure of MTJs. The cap layer has the structure of Ta(8 nm)/Ru(16 nm)/Ta (5 nm). (see supplementary information). For comparison purposes, micrometer size MTJs were fabricated by conventional photolithography & ion mill process[35] on the *exact same* wafers as those used in the NSL process, therefore the RA value could indicate the number of nanopillar under each cell.

Ordered nanopillar array fabrication. Ordered nanosphere lithography was carried out using a modified Langmuir-Blodgett monolayer deposition process[28]. Monolayer self-assembly took place in a 150 mL Teflon trough. The trough was filled with high purity DI water to the brim, and the pH was adjusted to be basic by the addition of NH_4OH solution. Adjusting the pH allows for the control of the number of dissociated functional groups on the nanospheres[28]. The nanosphere/ethanol solution (approx. 10–20 μL) was then slowly applied the water surface from a glass slide. In order to further facilitate self-assembly, polyethylene oxide (PEO) (Sigma-Aldritch MW = 100000 g/mol) was added via pipette so that the resulting concentration of PEO in the trough was 3–4ppm[39]. Some of the PEO diffused to the surface, forming a surfactant barrier which gently compressed the nanospheres on a time scale of minutes, while the remainder of the PEO remained in solution and screened the electrostatic repulsion between the nanospheres. PEO may also bond with the nanospheres, forming polymer "bridges" which improve the mechanical properties of the monolayer[39].

To transfer the monolayer to the MTJ film, the trough was slowly drained so that the water level dropped at a rate of 0.5 mm/s. The coated film was then removed and left to air dry. After that the size of the nanospheres was reduced by oxygen plasma. A low power density of 0.45 W/cm^2 was used to avoid overheating the nanospheres. Under this power density the size of nanospheres was reduced at 12.5 nm/min. Subsequently, ion beam etching was carried out and the dense array of nanopillars was formed after the liftoff of nanospheres.

Thermal annealing. Large TMR and proper magnetic anisotropy in these MgO-based MTJs can only be achieved after the post-growth thermal annealing. The MTJ nanopillars were annealed in a rapid thermal anneal (RTA) system for 10 min at 300°C. The temperature ramping rate of the RTA system is about 30°C/s. A magnetic field of 3–4 kOe has been applied during annealing, for samples with both in-plane and out-of-plane magnetic easy axis.

Magnetotransport measurement. The transport properties of the nanopillars with contact pads were measured in the conventional four-probe method. For the ordered MTJ arrays as shown in Figure 4, the resistance of the pillars was measured in the two-probe geometry. A sharp Tungsten tip was driven by a Newport NanoPZ Ultra-High Resolution Actuator, serving as the top electrode. The bottom electrode was connected to the MTJ film by Indium. The NanoPZ actuator is controlled by software and linear motion in steps as small as 10 nm can achieved (1 micro-step equals approximately 10 nm of linear motion). The motion of the NanoPZ was stopped when a sudden decrease of resistance (a few orders of magnitude) was detected. TMR curve was then recorded after each contact.

1. Moore, G. E. Cramming more components onto integrated circuits (Reprinted from Electronics, pg 114–117, April 19, 1965). *Proceedings of the IEEE* **86**, 82–85 (1998).
2. Pop, E. Energy dissipation and transport in nanoscale devices. *Nano Research* **3**, 147–169 (2010).
3. Wolf, S. A. *et al.* Spintronics: A Spin-Based Electronics Vision for the Future. *Science* **294**, 1488–1495 (2001).
4. Zutic, I., Fabian, J. & Das Sarma, S. Spintronics: Fundamentals and applications. *Rev. Mod. Phys. J1 - RMP* **76**, 323 (2004).
5. Moodera, J. S., Kinder, L. R., Wong, T. M. & Meservey, R. Large Magnetoresistance at Room-Temperature in Ferromagnetic Thin-Film Tunnel-Junctions. *Phys. Rev. Lett. J1 - PRL* **74**, 3273–3276 (1995).
6. Miyazaki, T. & Tezuka, N. Giant magnetic tunneling effect in Fe/Al2O3/Fe junction. *Journal of Magnetism and Magnetic Materials* **139**, L231–L234 (1995).
7. Parkin, S. S. P. *et al.* Giant tunnelling magnetoresistance at room temperature with MgO (100) tunnel barriers. *Nature Materials* **3**, 862–867 (2004).
8. Yuasa, S., Nagahama, T., Fukushima, A., Suzuki, Y. & Ando, K. Giant room-temperature magnetoresistance in single-crystal Fe/MgO/Fe magnetic tunnel junctions. *Nature Materials* **3**, 868–871 (2004).
9. Yuasa, S. & Djayaprawira, D. D. Giant tunnel magnetoresistance in magnetic tunnel junctions with a crystalline MgO(001) barrier. *J. Phys. D-Appl. Phys.* **40**, R337–R354 (2007).
10. Slonczewski, J. C. Current-driven excitation of magnetic multilayers. *Journal of Magnetism and Magnetic Materials* **159**, L1–L7 (1996).
11. Berger, L. Emission of spin waves by a magnetic multilayer traversed by a current. *Phys. Rev. B J1 - PRB* **54**, 9353–9358 (1996).
12. Ralph, D. C. & Stiles, M. D. Spin transfer torques. *Journal of Magnetism and Magnetic Materials* **320**, 1190–1216 (2008).
13. Sun, J. Z. & Ralph, D. C. Magnetoresistance and spin-transfer torque in magnetic tunnel junctions. *Journal of Magnetism and Magnetic Materials* **320**, 1227–1237 (2008).
14. Wang, W.-G., Li, M., Hageman, S. & Chien, C. L. Electric-field-assisted switching in magnetic tunnel junctions. *Nature Materials* **11**, 64 (2012).
15. Shiota, Y. *et al.* Induction of coherent magnetization switching in a few atomic layers of FeCo using voltage pulses. *Nat Mater* **11**, 39–43 (2012).
16. Butler, W. H., Zhang, X.-G., Schulthess, T. C. & MacLaren, J. M. Spin-dependent tunneling conductance of Fe|MgO|Fe sandwiches. *Phys. Rev. B J1 - PRB* **63**, 054416 (2001).
17. Katine, J. A., Albert, F. J., Buhrman, R. A., Myers, E. B. & Ralph, D. C. Current-Driven Magnetization Reversal and Spin-Wave Excitations in Co/Cu/Co Pillars. *Phys. Rev. Lett. J1 - PRL* **84**, 3149–3152 (2000).
18. Krivorotov, I. N. *et al.* Time-domain measurements of nanomagnet dynamics driven by spin-transfer torques. *Science* **307**, 228–231 (2005).
19. Mangin, S. *et al.* Current-induced magnetization reversal in nanopillars with perpendicular anisotropy. *Nature Materials* **5**, 210–215 (2006).
20. Boulle, O. *et al.* Shaped angular dependence of the spin-transfer torque and microwave generation without magnetic field. *Nature Physics* **3**, 492–497 (2007).
21. Ikeda, S. *et al.* A perpendicular-anisotropy CoFeB-MgO magnetic tunnel junction. *Nature Materials* **9**, 721–724 (2010).
22. Sun, J. Z., Monsma, D. J., Abraham, D. W., Rooks, M. J. & Koch, R. H. Batch-fabricated spin-injection magnetic switches. *Applied Physics Letters* **81**, 2202–2204 (2002).
23. Özyilmaz, B. *et al.* Current-Induced Magnetization Reversal in High Magnetic Fields in Co/Cu/Co Nanopillars. *Phys. Rev. Lett. J1 - PRL* **91**, 067203 (2003).
24. Huai, Y., Albert, F., Nguyen, P., Pakala, M. & Valet, T. Observation of spin-transfer switching in deep submicron-sized and low-resistance magnetic tunnel junctions. *Applied Physics Letters* **84**, 3118–3120 (2004).
25. Blamire, M. G., Aziz, A. & Robinson, J. W. A. Nanopillar junctions. *Philosophical Transactions of the Royal Society a-Mathematical Physical and Engineering Sciences* **369**, 3198–3213 (2011).
26. Haynes, C. L. & Van Duyne, R. P. Nanosphere Lithography: A Versatile Nanofabrication Tool for Studies of Size-Dependent Nanoparticle Optics. *The Journal of Physical Chemistry B* **105**, 5599–5611 (2001).
27. Hanarp, P., Sutherland, D. S., Gold, J. & Kasemo, B. Control of nanoparticle film structure for colloidal lithography. *Colloids and Surfaces A: Physicochemical and Engineering Aspects* **214**, 23–36 (2003).
28. Vogel, N., Weiss, C. K. & Landfester, K. From soft to hard: the generation of functional and complex colloidal monolayers for nanolithography. *Soft Matter* **8**, 4044–4061 (2012).
29. Zhu, F. Q. *et al.* Ultrahigh-Density Arrays of Ferromagnetic Nanorings on Macroscopic Areas. *Adv. Mater.* **16**, 2155–2159 (2004).
30. Sani, S. R., Persson, J., Mohseni, S. M., Fallahi, V. & Akerman, J. Current induced vortices in multi-nanocontact spin-torque devices. *Journal of Applied Physics* **109**, 07C913–913 (2011).
31. Wang, W. G. *et al.* In situ characterization of rapid crystallization of amorphous CoFeB electrodes in CoFeB/MgO/CoFeB junctions during thermal annealing. *Applied Physics Letters* **95**, 242501 (2009).
32. Wang, W. G. *et al.* Understanding tunneling magnetoresistance during thermal annealing in MgO-based junctions with CoFeB electrodes. *Phys. Rev. B J1 - PRB* **81**, 144406 (2010).
33. Wang, W. G. *et al.* Real-time evolution of tunneling magnetoresistance during annealing in CoFeB/MgO/CoFeB magnetic tunnel junctions. *Applied Physics Letters* **92**, 152501 (2008).
34. Wang, W.-G. *et al.* Rapid thermal annealing study of magnetoresistance and perpendicular anisotropy in magnetic tunnel junctions based on MgO and CoFeB. *Applied Physics Letters* **99**, 102502–102503 (2011).
35. Gallagher, W. J. *et al.* Microstructured magnetic tunnel junctions (invited). *Journal of Applied Physics* **81**, 3741–3746 (1997).
36. Kaka, S. *et al.* Mutual phase-locking of microwave spin torque nano-oscillators. *Nature* **437**, 389–392 (2005).
37. Mancoff, F. B., Rizzo, N. D., Engel, B. N. & Tehrani, S. Phase-locking in double-point-contact spin-transfer devices. *Nature* **437**, 393–395 (2005).
38. Ho, C.-C. *et al.* Reduced saturation magnetization in cobalt antidot thin films prepared by polyethylene oxide-assisted self-assembly of polystyrene nanospheres. *Applied Physics Letters* **96**, 122504–122503 (2010).
39. Ho, C. C., Chen, P. Y., Lin, K. H., Juan, W. T. & Lee, W. L. Fabrication of Monolayer of Polymer/Nanospheres Hybrid at a Water-Air Interface. *Acs Applied Materials & Interfaces* **3**, 204–208 (2011).
40. Worledge, D. C. & Abraham, D. W. Conducting atomic-force-microscope electrical characterization of submicron magnetic tunnel junctions. *Applied Physics Letters* **82**, 4522–4524 (2003).
41. Evarts, E. R. *et al.* Spin transfer torque switching of magnetic tunnel junctions using a conductive atomic force microscope. *Applied Physics Letters* **95**, 132510–132513 (2009).
42. Evarts, E. R. *et al.* Characterization of Conducting Atomic Force Microscopy for Use With Magnetic Tunnel Junctions. *Magnetics, IEEE Transactions on* **46**, 1741–1744 (2010).

43. Choi, Y. S. *et al.* Effect of Ta getter on the quality of MgO tunnel barrier in the polycrystalline CoFeB/MgO/CoFeB magnetic tunnel junction. *Applied Physics Letters* **90**, 012505–012503 (2007).

Acknowledgements
The authors would like to thank N. Vogel for generously providing us with nanosphere solutions and very helpful discussion. This work is supported by NSF DMR05-20491.

Author contributions
W.G.W. and C. L. C. conceived and designed the experiments. A. P., W.G.W., M.L., A. C., S. H. and F. Q. Z. worked on the deposition of nanospheres. M. L., S.H. and W.G.W. measured transport properties of the samples. C. L. C. supervised the study. W.G.W., C. L. C. and A. P. wrote the manuscript and all authors discussed the results and commented on the manuscript.

Additional information
Supplementary information accompanies this paper at http://www.nature.com/scientificreports

Competing financial interests: The authors declare no competing financial interests.

How to cite this article: Wang, W.G. *et al.* Parallel fabrication of magnetic tunnel junction nanopillars by nanosphere lithography. *Sci. Rep.* **3**, 1948; DOI:10.1038/srep01948 (2013).